Chemico-Biological Interactions 384 (2023) 110685

Contents lists available at ScienceDirect

Chemico-Biological Interactions

journal homepage: www.elsevier.com/locate/chembioint

Research paper

Cu(II)-acylhydrazone complex, a potent and selective antitumor agent against human osteosarcoma: Mechanism of action studies over *in vitro* and *in vivo* models

Lucia M. Balsa [a], Luisina M. Solernó [b,c], Maria R. Rodriguez [a], Beatriz S. Parajón-Costa [a], Ana C. Gonzalez-Baró [a], Daniel F. Alonso [b], Juan Garona [b,c], Ignacio E. León [a,d,*]

[a] CEQUINOR (UNLP, CCT-CONICET La Plata, Asociado a CIC), Departamento de Química, Facultad de Ciencias Exactas, Universidad Nacional de La Plata, Blvd. 120 N° 1465, La Plata, 1900, Argentina
[b] Centro de Oncología Molecular y Traslacional (COMTra), Universidad Nacional de Quilmes, Argentina
[c] Centro de Medicina Traslacional (Unidad 6), Hospital de Alta Complejidad en Red El Cruce "Dr. Néstor Carlos Kirchner" S.A.M.I.C, Argentina
[d] Cátedra de Fisiopatología, Departamento de Ciencias Biológicas, Facultad de Ciencias Exactas, Universidad Nacional de La Plata, 47 y 115, La Plata, 1900, Argentina

ARTICLE INFO

Keywords:
Cancer
Osteosarcoma
Copper complexes
Mechanism of action
Proteomic approach
In vivo studies

ABSTRACT

Osteosarcoma (OS) is a frequent bone cancer, affecting largely children and young adults. Cisplatin (CDDP) has been efficacious in the treatment of different cancer such us OS but the development of chemoresistance and important side effects leading to therapeutic failure. Novel therapies including copper compounds have shown to be potentially effective as anticancer drugs and one alternative to usually employed platinum compounds.

The goal of this work is the evaluation of the *in vitro* and *in vivo* antitumoral activity and dilucidate the molecular target of a Cu(II) cationic complex containing a tridentate hydrazone ligand, CuHL for short, H_2L=N'-'-(2-hydroxy-3-methoxybenzylidene)thiophene-2-carbohydrazide, against human OS MG-63 cells.

Anticancer activity on MG-63 cell line was evaluated in OS monolayer and spheroids. CuHL significantly impaired cell viability in both models (IC_{50} 2D: 2.1 ± 0.3 μM; 3D: 9.1 ± 1.0 μM) ($p < 0.001$). Additional cell studies demonstrated the copper compound inhibits cell proliferation and conveys cells to apoptosis, determined by flow cytometry. CuHL showed a great genotoxicity, evaluated by comet assay. Proteomic analysis by Orbitrap Mass Spectometry identified 27 differentially expressed proteins: 17 proteins were found overexpressed and 10 underexpressed in MG-63 cells after the CuHL treatment. The response to unfolded protein was the most affected biological process.

In addition, *in vivo* antitumor effects of the compound were evaluated on human OS tumors xenografted in nude mice. CuHL treatment, at a dose of 2 mg/kg i.p., given three times/week for one month, significantly inhibited the progression of OS xenografts and was associated to a reduction in mitotic index and to an increment of tumor necrosis ($p < 0.01$). Administration of standard-of-care cytotoxic agent CDDP, following the same treatment schedule as CuHL, failed to impair OS growth and progression.

1. Introduction

Cancer is one of the main causes of death worldwide [1]. Particularly, osteosarcoma (OS) is a high-grade bone malignancy that signifies the most common primary bone cancer in children and young adults [2]. This type of cancer has special features such as the deposition of immature osteoid matrix by highly proliferating and invasive cells.

Currently, the therapeutic strategy in the treatment of OS involves surgery and pre-and postoperative chemotherapy. These regimens include a combination of methotrexate, doxorubicin, and cisplatin (CDDP), or etoposide in addition to ifosfamide [3]. However, despite the use of combination therapy, approximately 40% of OS patients develop local recurrences or distant metastases showing elevated mortality rates [4]. Besides, in high-income countries the 5-year survival rates of up to 70% whilst in low- and middle-income countries this rate is significantly lower, with reported survival rates as low as 45% [5].

* Corresponding author. CEQUINOR (UNLP, CCT-CONICET La Plata, Asociado a CIC), Departamento de Química, Facultad de Ciencias Exactas, Universidad Nacional de La Plata, Blvd. 120 N° 1465, La Plata, 1900, Argentina.
E-mail address: ileon@biol.unlp.edu.ar (I.E. León).

https://doi.org/10.1016/j.cbi.2023.110685
Received 16 May 2023; Received in revised form 5 August 2023; Accepted 26 August 2023
Available online 4 September 2023

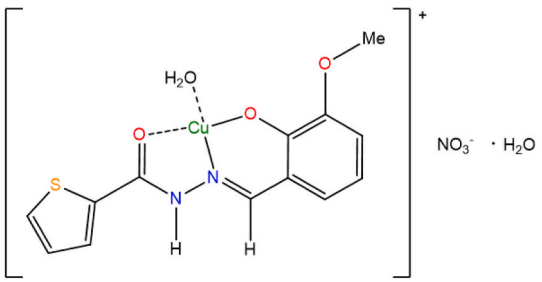

Fig. 1. Schematic representation of CuHL.

Table 1
IC_{50} values of copper-hidrazones complexes (CuHL, [$CuHL^1$], [$Cu(L^1)$(*o*-phen)], [$Cu(HL^1)$(bipy)](NO_3)), ligand (H_2L), free metal cation (Cu^{2+}). and CDDP on MG-63 cells (2D) and spheroids derived from MG-63 cells (3D) after 24 h of incubation.

	2D	3D	Reference
CuHL	2.1 ± 0.3	9.1 ± 1.0	This work
H_2L	>100.0	n.d	This work
$Cu^{(2+)}$	>100.0	n.d	This work
CDDP	39.0 ± 1.80	65.1 ± 5.6	[32]
[$CuHL^1$]	10.7 ± 1.6	n.d	[27]
[$Cu(L^1)$(*o*-phen)]	3.5 ± 0.3	n.d	[33]
[$Cu(HL^1)$(bipy)](NO_3)	5.6 ± 1.0	n.d	[33]

Taking into account that therapeutical advances of OS and survival rates have reached a discouraging plateau, there is a relevant need to identify novel therapeutic alternatives for the treatment of OS. Metallodrugs are a class of anticancer compounds mostly used in the treatment of different types of tumors including breast, colorectal, lung, and bone cancer [6,7]. In this way, platinum complexes, specifically CDDP, carboplatin, and oxaliplatin, are successfully used in the clinical approach of many oncological patients [8], but inherent and acquired resistance to platinum drugs is one of the most related clinical problems in the treatment [9]. Therefore, novel non-platinum-based compounds including ruthenium, vanadium, and copper complexes have appeared as alternatives to the use of platinum in clinical cancer therapy [6,10,11]. Particularly, copper complexes have shown interesting *in vitro* and *in vivo* anticancer effects over various cancer cell models [12–17]. One of the most important mechanisms of action reported about copper complexes involves ROS generation, and consequent DNA damage [18–20]. Besides, proteasome inhibition activity and cancer stem cells are reported as two important mechanisms of cell death activated by copper compounds [21,22]. Furthermore, different copper complexes showed stronger anticancer activity than their ligands which suggest the key role of the metal itself in the anticancer actions [14,23,24]. However, only a few copper complexes showed remarkable anticancer activity against OS cells [25–27].

Due to the high mortality of OS and the limited effectiveness of current therapeutic options, this research deals with the *in vitro* and *in vivo* antitumor properties and the mechanism of action of [Cu(HL)(OH_2)] (NO_3). H_2O complex (henceforth referred to as "CuHL", for simplicity), where H_2L = [H_2L=N'-(2-hydroxy-3-methoxybenzylidene) thiophene-2-carbohydrazide], on 2D, 3D and xenograft OS tumor models. Our study aimed to explore CuHL target expression, DNA damage, and induction of apoptosis in OS cells. Moreover, we focused our research on evaluating the effect of sustained CuHL administration in OS tumor progression.

2. Materials and methods

2.1. Synthesis, identification and preparation of CuHL

The copper compound was obtained following the procedure described in our previous work [28].

CuHL stock solutions (20 mM) were prepared in dimethylsulfoxide (DMSO) and forward diluted according to the concentrations used in each experiment. Maximum concentration of DMSO was kept at 0,5%. CDDP was dissolved on normal saline solution (0.9% w/w).

2.2. Cell line and growing conditions

Human OS MG-63 cell line (ATCC CRL-1427 ™) was grown in Dulbecco's modified Eagle's medium (DMEM) containing 10% fetal bovine serum (FBS), 100 IU/mL penicillin and 100 μg/mL streptomycin at 37 °C in 5% CO_2 atmosphere.

Table 2
Percentage of early and late apoptotic cells after treatment with CuHL. *p < 0.01 Differences between control and treatment.

	ANV+/PI-	ANV+/PI+	ANV-/PI+
0	1.1 ± 0.4	5.3 ± 2.6	0.8 ± 0.3
0.5	1.6 ± 0.1	4.0 ± 0.3	0.3 ± 0.1
1	5.6 ± 1.0 *	16.5 ± 0.4 *	0.7 ± 0.1
2.5	2.9 ± 0.5 *	58.2 ± 0.1 *	4.3 ± 0.7

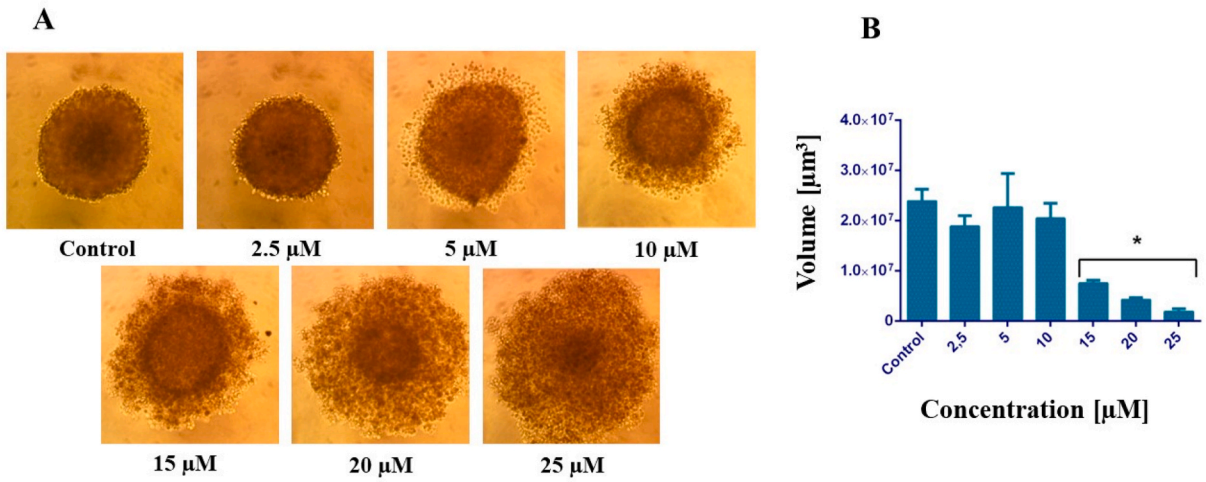

Fig. 2. A) Images of MG-63 spheroids after the treatment with 2.5–25 μM of CuHL. B) Graph bars of volume derived from spheroids.

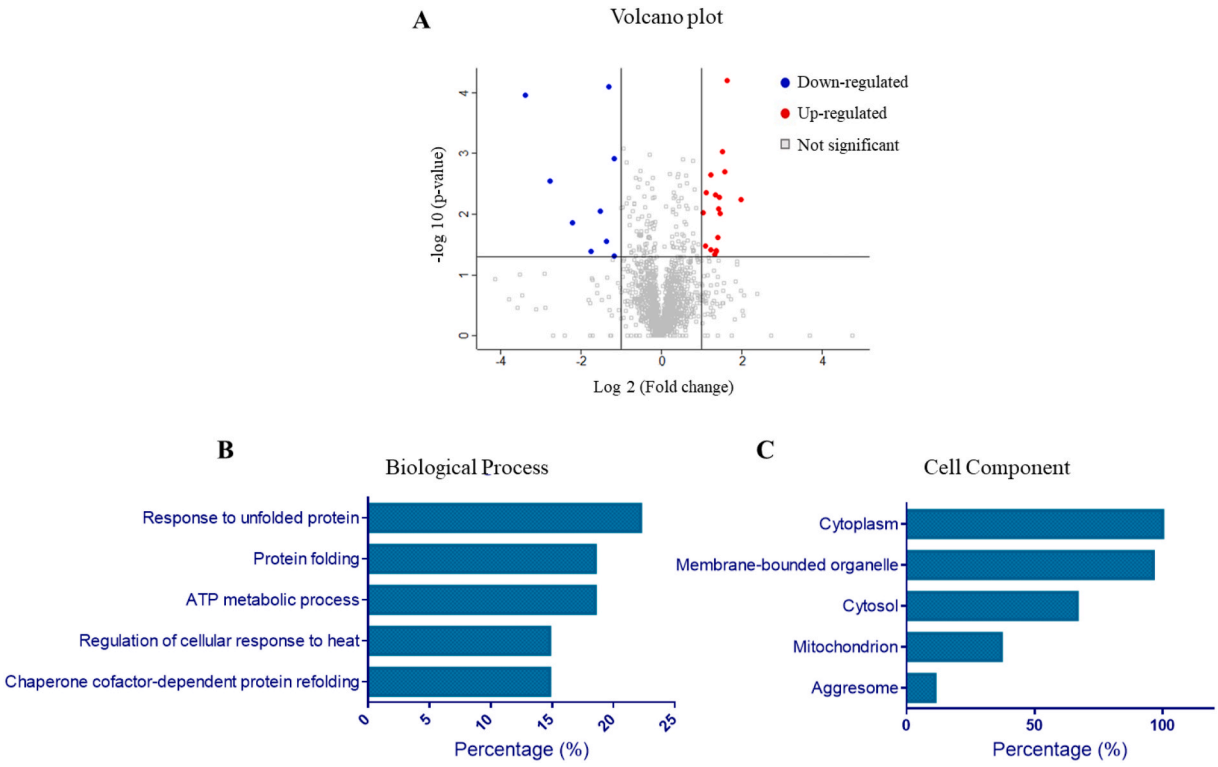

Fig. 3. A) Volcano plot illustrates significantly differentially abundant proteins (down regulated in blue and up-regulated in red) after treatment with CuHL. The log10 (Student T-test P value) is plotted against the log2 (fold change: Treatment CuHL/Control). The non-axial vertical lines denote ±2-fold change while the non-axial horizontal line denotes P = 0.05, which is our significance threshold (prior to logarithmic transformation). **B)** Biological processes. **C)** Component associated with the up and down proteins identified after CuHL treatment in MG-63 cells. Results obtained with STRING.

Table 3
Ingenuity canonical pathways associated with differentially expressed proteins after CuHL treatment. Results obtained with the IPA tool.

Canonical pathways	-LOG(p-value)	Proteins
UNFOLDED PROTEIN RESPONSE	5.47	DNAJB1, DNAJB4, HSPA1A/HSPA1B, HSPH1
ALDOSTERONE SIGNALING IN EPITHELIAL CELLS	4.4	DNAJB1, DNAJB4, HSPA1A/HSPA1B, HSPH1
PROTEIN UBIQUITINATION PATHWAY	3.58	DNAJB1, DNAJB4, HSPA1A/HSPA1B, HSPH1
OXIDATIVE PHOSPHORYLATION	3.55	ATP5PO, COX5A, SDHA
TRNA CHARGING	3.03	AARS2, CARS2
MITOCHONDRIAL DYSFUNCTION	3.01	ATP5PO, COX5A, SDHA

2.3. Cell viability study

MG-63 cells were seeded in a 96-multiwell dish and treated with different concentrations of compounds (CuHL and CDDP) at 37 °C for 24 h. Then, medium was changed and cells were incubated with 0.2 mg/mL of the resazurin for 6 h.

2.4. Clonogenic assay

After attachment of the cells to the 24 multiwell plates and the treatment with CuHL at a range of 0.125–0.5 μM, the cells were washed with PBS and added with complete DMEM (2 mL). Then, the 24-multiwell were incubated for 10 days at 37 °C and 5% CO_2. Next, medium was removed and cells were stained (6% of glutaraldehyde and 0.5% crystal violet) for 30 min at room temperature. Afterward, we proceed to count the colonies. The plating efficiency (PE) was calculated as a ratio of the number of colonies to the number of cells seeded whilst the surviving fraction (SF) is defined as the number of colonies that survive after the treatment, expressed in terms of PE.

2.5. Apoptosis

Apoptosis was detected using Annexin V-FITC and propidium iodide (PI) staining and following the procedure published in our preceding manuscript [14].

Cells were analyzed using a flow cytometer BD Accuri C6 Plus and BD Accuri C6 Plus software.

2.6. Single cell gel electrophoresis (SCGE) assay

DNA damage were achieved following the method of Singh et al. with minor modifications [29]. Cellular images were acquired with the Leica IM50 Image Manager (ImagicBildverarbeitung AG). The tail moment (product of tail length by tail DNA percentage) was determined with 50 randomly captured cells and using a free comet scoring software (Comet Score version 1.5).

2.7. Proteomic analysis

2.7.1. Protein sample preparation

For sample preparation, MG-63 cells were seeded in a 6-well dish, allowed to attach for 24 h, and treated with 1 μM of the complex at 37 °C. Total protein was extracted from MG-63 cells after 24 h. Briefly, cells were homogenized in RIPA lysis buffer containing a protease inhibitor cocktail. Then, total protein was collected through centrifugation at 12,000 g for 20 min at 4 °C, and protein concentration was determined using BCA protein assay.

2.7.2. Protein identification and mass spectrometry

Samples were sent to the Center for Chemical and Biological Studies

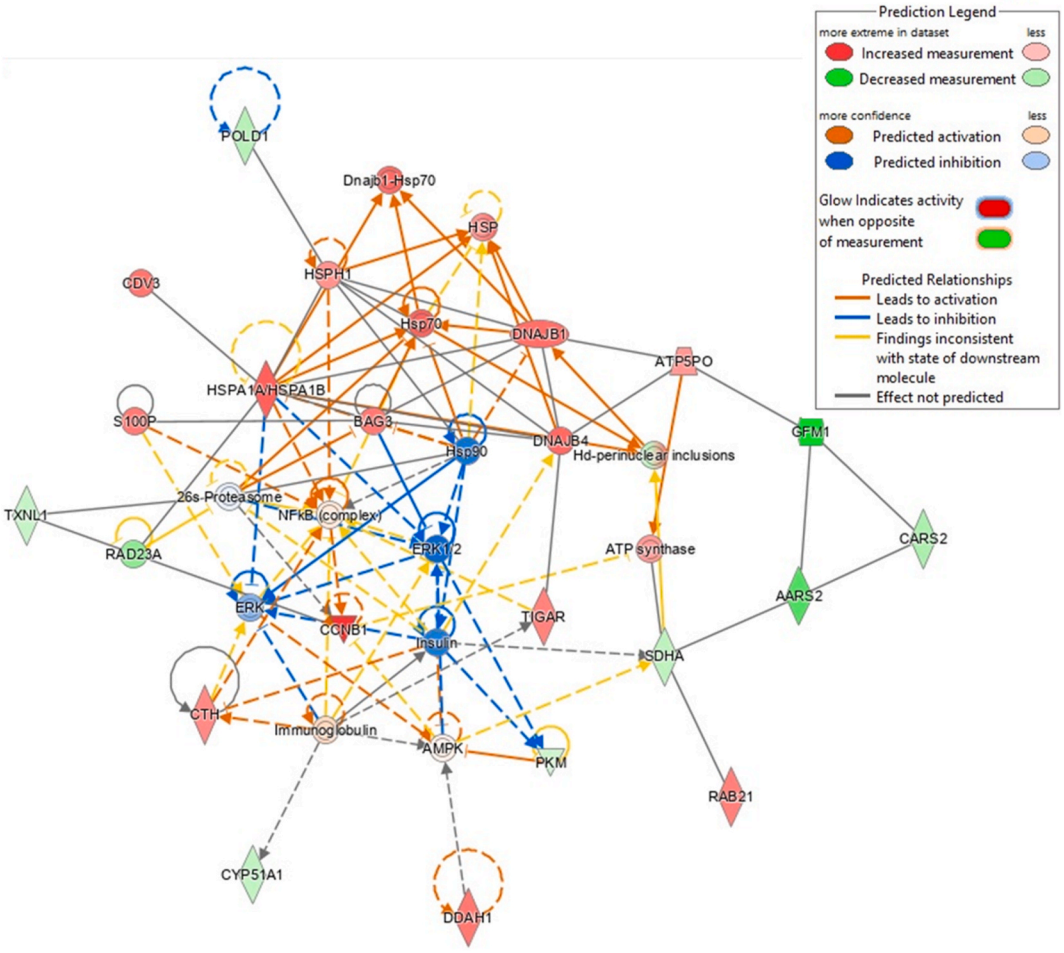

Fig. 4. Scheme of the protein's connection networks obtained using IPA.

by Mass Spectrometry (CEQUIBIEM), for Label Free Quantification analysis. In brief, samples were reduced with DTT, alkylated with iodoacetamide followed by trypsin digestion. Samples were lyophilized by Speed Vac and resuspended in 0.1% trifluoroacetic acid. Then, liquid chromatography was performed with nanoHPLC Easy nLC 1000 (Thermo Scientific) coupled to a mass spectrometer with Orbitrap technology (Thermo Scientific), which allows separation and further identification of the peptides.

Analysis of the spectra obtained by the mass spectrometer was performed using the Proteome Discoverer search engine with the *Homo sapiens* database. For the search, the following parameters were set: trypsin was used as the cleavage protease; two missed cleavage was allowed; the precursor peptide mass tolerance was set at 10 ppm while fragment mass tolerance was 0.05 Da; carbamidomethylation (C) was set as a fixed modification; variable modification was set to oxidation; minimum identification criteria required a minimum of 2 peptides per protein.

Statistical analysis for differentially expressed proteins was performed using the software Perseus v.1.6.6.0. The *t*-test was used to compare protein abundance averages between treatment and control groups. Differentially expressed proteins were identified when: *t*-test p value < 0.05 and there was an increase or decrease in protein level of 2-fold or more.

2.7.3. Bioinformatics analysis

The differentially expressed proteins were used to perform protein–protein interaction (PPI) network construction and Gene Ontology (GO) enrichment analysis with the Search Tool for the Retrieval of Interacting Genes (STRING) database. Significantly enriched pathways were identified by searching against KEGG (Kyoto Encyclopedia of Genes and Genomes) and REACTOME databases.

2.8. Multicellular spheroids development

Multicellular tumor spheroids were formed with M6-63 cells using the adapted hanging drop method previously published with us [30].

Multicellular spheroids derived from MG-63 cells were treated in 96-well plates with 0.5% DMSO in DMEM (control) and with CuHL (0.5–25 μM) and CDDP (0.5–100 μM) in a range of concentration for 24 h. Then, cell viability was also determinate using resazurin.

Size and morphology of spheroids were evaluated and recorded using an inverted microscope (Olympus BX51) with a digital camera (AmScope) and ImageJ version 1.51n software. From the obtained images, spheroid boundaries were marked with the polygon tool of ImageJ. The measurement tool was used to determine the projected Area, Feret's diameter and shape descriptors of spheroids. Particles of known size were used for calibration. The volume was calculated from the obtained radius: $V = 4/3\ \pi\ r3$.

2.9. In vivo OS tumor growth

8 weeks old outbred female N:NIH(S)-nu mice were housed in the National University of Quilmes animal facility (5–6 animals per cage), with free access to water and food. Animals were acquired from the Animal Facility of the School of Veterinary Sciences at the National University of La Plata, Buenos Aires. A cell suspension containing 100 μL

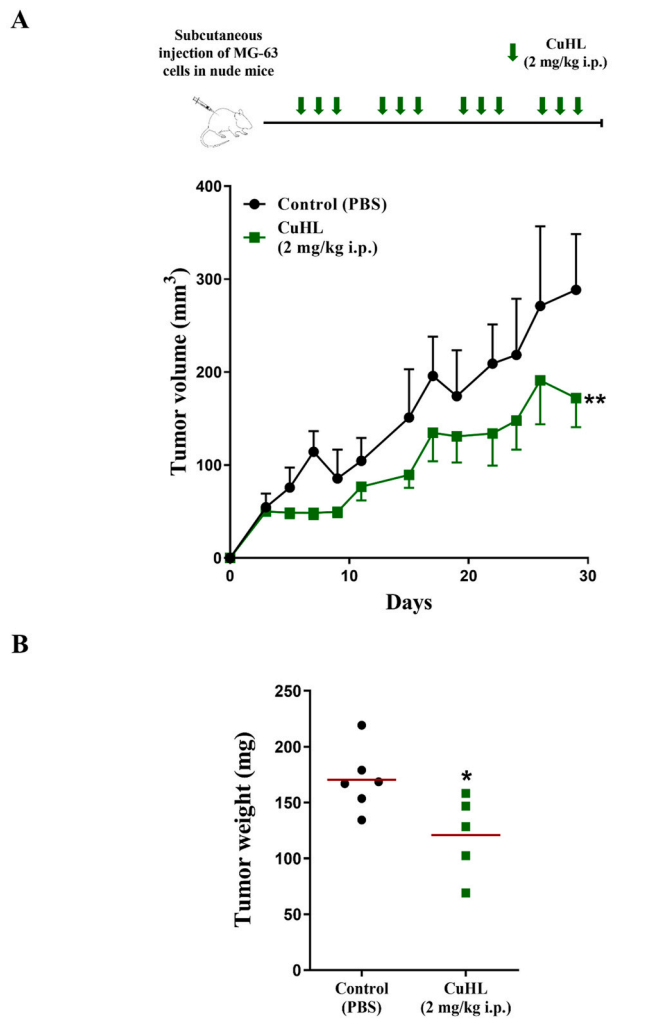

Fig. 5. A) In vivo activity of CuHL, administered using a 2 mg/kg i.p. dose, on human OS MG-63 xenograft progression in N:NIH(S) nude mice. Curves represent mean tumor volumes of mice receiving PBS (black) or CuHL (green). On top, the experimental design of the in vivo protocol is depicted. 5 or 6 female mice per group. Comparisons between experimental groups were performed by contrasting tumor growth rates. **B)** Tumor burden was additionally assessed by weighing OS primary lesions after necropsy and tumor recovery. Values as mean ± SEM. *p < 0.05, **p < 0.01, unpaired *t*-test.

of DMEM plus 50 μL Matrigel® (Becton Dickinson), and 5×10^6 MG-63 human OS cells was injected s.c. in the right flank of nude mice in order to produce tumor implants. After tumor cell injection, animals were grouped randomly into a control group (saline vehicle) and CuHL treatment group.

Xenograft growth was assessed using a caliper two times per week. Volume calculation was conducted by the following equation "0.52 x W^2 x L", where W = width, and L = length. Tumor growth rates (TGR) for each experimental condition were assessed and were calculated as the linear regression slopes of the xenograft volumes throughout time (between days 5 and 29). Treatment with CuHL (2 mg/kg i.p.) began 4 days after tumor challenge, once all engraftments were confirmed by palpation. Compound was administered 3 times/week for 4 weeks in total. The weight of experimental animals was additionally recorded throughout the assay, from day 4 (before treatment) until necropsy at day 31. Reference cytotoxic agent CDDP was used at an equivalent dose of 2 mg/kg i.p., also following a treatment schedule of 3 times/week for 4 weeks.

When primary tumors reached a volume of 300 mm^3 and started showing ulceration and signs of skin invasion, animals were sacrificed by cervical dislocation. Mice were photographed before sacrifice and protocol termination. OS tumors were recovered, fixed with buffered formalin and processed for hematoxylin and eosin staining.

2.10. Histopathological studies in OS xenografts

First, assessment of tumor mitotic indexes in xenografts belonging to vehicle- or CuHL-treated animals was performed using viable sections of tissue slides after hematoxylin and eosin staining. Quantification of mitotic bodies was conducted in randomly-selected X400 high power fileds. Histopathological analysis and findings were performed and confirmed by two blinded researchers, respectively. Second, color brightfield images of entire tissue sections stained with hematoxylin and eosin were acquired at ×2.5 magnification for tumor necrosis analysis. Images were taken with a Cytation Gen5 Reader (BioTek). The "Image Montage" function was used in order to performed stitching with a 10% tile overlapping. Tumor necrosis in OS tissue slides was detected in 4 sections per treatment group as areas with a marked increase of eosinophilia and was measured with the ImageJ 1.5j8 Software (NIH), by using the "Color Threshold'' tool. Tumor necrotic rates (TNR) for control and CuHL xenografts were determined following the equation TNR = (NA x 100)/(VA + NA), in which VA = viable area, and NA = necrotic area. Necrotic areas were adjusted to changes in tumor sizes by using the formula ATNR = 100 - (100 - TNR) x RTGR, where RTGR = group-specific relative tumor growth rates, and ATNR = adjusted tumor necrotic rates. RTGR was determined after transforming TGR values (Control 8.6 ± 0.8, and CuHL 6.0 ± 1.0 mm^3/day), taking the TGR of the control group as "1".

2.11. Toxicological studies

In order to perform further hematological and biochemical analysis, and before ending the in vivo protocol and sacrificing the animals, mice were anesthetized with a ketamine and xylazine mixture (100 mg/kg and 10 mg/kg xylazine, respectively, both i.p.) and whole-blood samples were collected in EDTA-coated tubes. Levels of cholesterol, direct bilirubin, creatinine, albumin and total protein were determined, as well as aspartate aminotransferase and alanine aminotransferase activity. Platelet, hematocrit, red and white blood cell counts, were also performed. Additionally, after euthanasia, kidneys, brain and liver were recovered, fixed and processed for histopathological assessment, after hematoxylin and eosin staining.

2.12. Ethics statements

Protocols using experimental animals were evaluated and approved by the National University of Quilmes Animal Care Committee (Resolution UNQ CyT-CICUAL CD075-14); Protocol number 011–15. Findings from in vivo protocols were reported according to the ARRIVE guidelines. Assays were carried out in accordance with the Guide for the Care and Use of Laboratory Animals (NIH Publications No. 8023; Rev. 1978).

2.13. Statistical analysis

Three independent experiments were achieved and the results are expressed as mean ± standard error of the mean (SEM), unless stated otherwise. The variance method followed by the test (Fisher) were used to analyzed the statistical differences.

Mann Whitney and *t* tests were used for non-parametric and normal distribution of data. Differences were considered statistically significant at a level of $p < 0.05$. The statistical analyses were performed using STATGRAPHICS Centurion XVI.I or GraphPad Prism v6.0.0 (GraphPad Software Inc., www.graphpad.com).

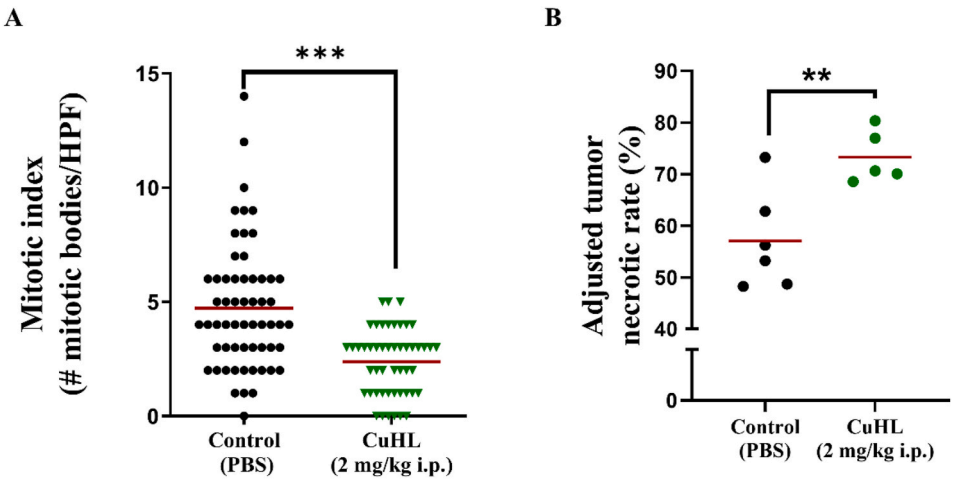

Fig. 6. A) Mitotic index assessment in OS tumor sections from control or CuHL-treated mice. Data was expressed as the number of mitotic bodies/HPF. **B)** Necrosis in primary OS lesions was also evaluated after treatment with saline vehicle or CuHL, and shown as adjusted tumor necrotic rates. Values as mean ± SEM. **p < 0.01, ***p < 0.001, Mann Whitney and unpaired *t*-test, respectively.

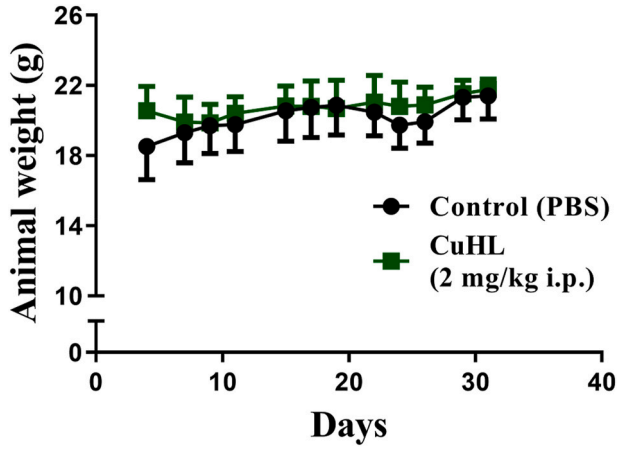

Fig. 7. Animal weight of control or CuHL-treated nude mice bearing OS xenografts were monitored throughout the in vivo assay to discard toxicity of CuHL treatment.

3. Results

3.1. Synthesis and characterization of CuHL

The compound was designed, synthetized and characterized following the procedure described in our previous work [28].

The structure of the CuHL is schematized in Fig. 1. Besides, the CuHL is stable over time on biological medium and DMSO [14].

3.2. CuHL inhibits cell viability and cell proliferation on 2D and 3D OS cancer cell models

Cytotoxicity studies for CuHL, H_2L and copper nitrate on human OS MG-63 cell line were performed using CDDP as a reference of anticancer clinical drug.

The results show that CuHL decreases the cell viability in the low micromolar concentration range (1–5 μM) on MG-63 cells exhibiting an IC_{50} value of 2.1 ± 0.3 μM ($p < 0.01$). To verify the important role of metal complexation, we checked the anticancer activity of ligand (H_2L) and free metal cation (Cu^{2+}). The results showed that ligand and free metals are not active in MG-63 cells with IC_{50} values higher than 100 μM demostrating the key rol of complexation in the enhancement of the

Table 4
Biochemical and general hematological parameters in mice after sustained treatment with CuHL in comparison to vehicle-treated (control) animals.

	Parameters										
	Weight (g)	Hematocrit (%)	RBC (10^6/mL)	WBC (10^3/mL)	Cholesterol (mg/dl)	Total protein (g/dl)	Direct bilirubin (mg/dl)	Creatinine (mg/mL)	GOT (IU/l)	ALT (IU/l)	Plasmatic Albumine (g/dl)
Control	21.40 ± 1.32	38.67 ± 1.86	72.58 ± 4.30	2.87± 1.04	81.17 ± 13.51	4.21± 0.40	0.02± 0.01	0.13± 0.04	135.7± 16.33	40.17 ± 11.48	2.52± 0.18
CuHL	21.76 ± 0.59	39.25 ± 2.22	72.00 ± 4.68	1.83± 0.64	87.00 ± 18.20	3.94± 0.69	0.01± 0.01	0.13± 0.06	191.8± 62.38	68.75 ± 46.02	2.64± 0.38

RBC; red blood cells. WBC; white blood cells. GOT; aspartate aminotransferase. ALT; alanine aminotransferase. IU; international units.

Table 5
Absolute leukocyte count in mice after sustained treatment with CuHL in comparison to vehicle-treated (control) animals.

	Absolute leukocyte count					
	Band neutrophils	Segmented neutrophils	Eosinophils	Basophils	Lymphocytes	Monocytes
Control	0.0 ± 0.0	238.8 ± 204	0.0 ± 0.0	56.5 ± 39.7	2410 ± 866.3	102.4 ± 47.3
CuHL	0.0 ± 0.0	61.5 ± 63	2.25 ± 6.5	131.±88.3	1567 ± 583.9	17.3 ± 7.5**

**p < 0.01. T-test control versus CuHL.

anticancer activity of CuHL (Table 1). The beneficial effects of complexation were reported for other metallodrugs and their respective ligands and free metals [15,16,31].

Moreover, the IC_{50} of CDDP is 39 ± 1.80 so CuHL is much more active than CDDP showing an IC_{50} value around 20-fold lower on MG-63 cells.

To further characterize the anticancer activity of our copper complex, we evaluated CuHL and CDDP effects on the cell viability of MG-63 multicellular spheroids. Table 1 shows that the IC_{50} value for CuHL is 9.1 ± 1.0 μM while for CDDP is 65.1 ± 5.6 μM showing an IC_{50} value 7-fold lower than CDDP toward OS multicellular spheroids. Besides, as it can be seen in Fig. 2, CuHL impaired 3D cell growth affecting the shape and volume of the spheroids.

On the other hand, we evaluated the effect of CuHL on the colony-forming ability of OS cells using a clonogenic study. Figure SM1 showed a notable reduction over clonogenic cell growth of MG-63 cells in a dose-dependent manner, from 0.125 to 0.5 μM ($p < 0.01$) suggesting the potential antiproliferative effects of CuHL.

3.3. CuHL induces apoptosis and DNA damage

The process of apoptosis is characterized by biochemical changes and morphological features and enhanced by harmful agents [34]. The externalization of phosphatidylserine is a relevant marker of earlier apoptotic events and annexin V is extensively used to quantify the apoptotic levels [35]. Commonly, metal-based drugs induce apoptosis as a mechanism of cell death [32,36].

Table 2 and Figure SM2 show the flow cytometry results of the apoptotic process after incubation of CuHL (0.5, 1.0 and 2.5 μM) on MG-63 cells. CuHL provoked an increment on the early (Annexin V+/PI-) and late (Annexin V+/PI+) apoptotic OS cell populations at 1.0 and 2.5 μM.

At 1 μM of CuHL, the fractions of Annexin V+/PI- cells increased severely from 1.1% (control) to 5.6%, whilst the Annexin V+/PI+ populations increased from 5.3% to 16.5%. Besides, after incubation with 2.5 μM of CuHL, the Annexin V+/PI- cells fraction increased to 2.9% compared with untreated condition (1.1%) and the % of Annexin V+/PI + cells was 58% vs 5% of the control condition.

Moreover, changes in the necrotic cell population (Annexin V-/PI+) were not observed with the incubation of CuHL. These results are in concordance with the cell viability and cell proliferation studies, suggesting that this complex induces OS cell apoptosis depending on its concentration. It is relevant to remark that programmed cell death has also been defined as the main mechanism of death for different copper compounds on various cancer cell lines [6,13].

The induction of DNA damage of CuHL was studied using the comet assay. The tail moment (tail length × DNA amount in the tail) analysis showed that CuHL induced an important genotoxic effect on MG-63 cells in the range of concentrations between 0.5 and 1.5 μM ($p < 0.01$). The tail moment values on MG-63 cells are 8.9 ± 1.9 (basal condition, 0 μM CuHL), 59.8 ± 6.0 (0.5 μM CuHL), and 145.6 ± 11.4 (1.0 μM CuHL) evidencing the DNA damage induced by copper(II) complex. Similar results were published about the interaction of DNA with copper(II)-hidrazones complexes in breast cancer cells showing an equivalent tail moment [14,16,37].

3.4. Deciphering molecular targets of CuHL using proteomics approaches

With the aim to elucidate novel molecular targets and cell pathways activated or inactivated by CuHL, we performed an LFQ assay using mass spectrometry (MS).

As a result of these studies, 27 proteins were identified: 17 proteins were found overexpressed and 10 underexpressed on MG-63 cells after the treatment with 1 μM of CuHL (Fig. 3A). The symbol of the gene encoding each protein, the name of these proteins, a brief protein functional description, fold change and the p-value associated with each protein are included in Table SM1.

To study and explore the biological characteristics of the 27 differentially expressed proteins found after the CuHL treatment, a set of bioinformatics approaches were used. In this way, proteins were classified using the STRING database by means of the biological processes in which they were involved (Fig. 3B) and the cell components (Fig. 3C).

As a result, "response to unfolded protein" was the most affected biological process (22.2%). Other substantially affected processes were “regulation of cellular response to heat", "chaperone cofactor-dependent protein refolding” and “ATP metabolic processes”, among others (Table SM2). Additionally, “cellular component” was also analyzed by STRING. Fig. 3C and Table SM3 show that cytoplasm represented a 100% of totally proteins whilst mitochondrion and aggresome represented a 37% and 11%, respectively.

To confirm the findings showed in Table 3 we used the ingenuity pathway analysis (IPA) bioinformatics tool. Table 3 shows the six most affected canonical pathways after treatment with CuHL in MG-63 cells. The results are in agreement with the STRING analysis.

Particularly, the most altered pathways listed in IPA were unfolded protein response including Heat Shock proteins (HSPA1A/HSPA1B, HSPH1) and DNAJ homolog subfamily members that stimulate the ATPase activity of HSP. Aldosterone Signaling in Epithelial Cells and Protein Ubiquitination Pathway were included in 2nd and 3rd positions and are involved the same protein family that unfolded protein response. The protein ubiquitination pathway controls the degradation of cellular proteins through the ubiquitin-proteasome system, monitoring protein’s half-life and expression levels as well as vital cellular processes [38]. Moreover, relevant cellular functions are regulated by the other canonical pathways identified by the IPA tool, such as cell growth and metabolism (oxidative phosphorylation), cell death (mitochondrial dysfunction) [39], and oncogenesis (Trna charging). Fig. 4 shows a network of molecules (type of connection) and the function of these molecules designed with IPA.

3.5. CuHL inhibits OS growth in vivo

With the aim of assessing potential therapeutic benefits of CuHL on OS progression, its activity was evaluated on MG-63 xenografts growing in nude mice. Novel metallodrug was administered i.p., three times/week, at a dose of 2 mg/kg after tumor engraftment confirmation. After four weeks of treatment, CuHL treatment was associated to a significant reduction in tumor volume (control 288.5 ± 60.1 versus CuHL 172.1 ± 69.9; mean ± SD), causing a tumor growth inhibition of 40.3% in contrast to PBS-treated animals (Fig. 5A). Impact of sustained CuHL administration on tumor burden was confirmed after observing a 29% reduction in the weight of resected primary tumors (control 170.4 ± 28.5 mg versus CuHL 121.0 ± 35.9 mg; mean ± SD) (Fig. 5B). Besides measuring tumor diameters for tumor volume and growth rate calculation, general health status and well-being of experimental animals was also assessed over time. All animals receiving CuHL at 2 mg/kg i.p. dose (3 times per week) survived the complete 4 week-treatment schedule. Treatment was well tolerated given that no changes in animal body weight, behaviour, food or water consumption were observed throughout the *in vivo* protocol.

Representative photographs of OS xenograft-bearing animals from control or CuHL groups are shown in Figure SM3. Additionally, the administration of standard-of-care cytotoxic agent CDDP, following the same treatment schedule as CuHL, failed to impair OS growth and progression (Figure SM4). Taking into account its prognostic value in cancer patients and its association with OS aggressiveness, mitotic indexes were quantified in MG-63 lesions obtaining values of 4.7 ± 2.7 and 2.4 ± 1.4 (mean ± SD) mitotic bodies/HPF (high-power field) for control and CuHL, respectively (Fig. 6A and Figure SM5). Necrosis was also assessed in OS xenografts after treatment by adjusted tumor necrotic rate (ATNR) calculation. CuHL-based therapy notoriously enhanced ATNR in contrast to PBS-treated mice, from 57.1 ± 9.6 to 73.3

± 5.1%, respectively (Fig. 6B and SM6).

No changes in food or water consumption, nor in animal weight, were associated to sustained CuHL administration (Fig. 7). Isolated regions of acute tubular necrosis were detected in renal tissue. No histopathological alterations or signs of toxicity were observed in liver or brain tissue (Figure SM7). Biochemical and Hematological values after 4 weeks of CuHL treatment are displayed in Tables 4 and 5. Non-significant increases in alanine aminotransferase and aspartate aminotransferase levels were observed in CuHL-treated animals. Total protein, creatinine and bilirubin levels remain unaltered (Table 4). A notorious decrease in the number of monocytes was observed in CuHL-treated mice (102.4 ± 47.2 versus 17.3 ± 7.5 for control and CuHL, respectively). Complex administration was also associated with non-significant increased numbers of basophils (56.5 ± 39.7 versus 181 ± 88.3, for control and CuHL, respectively) (Table 5).

4. Discussion

The antitumor effects and the mechanism of action of CuHL were studied *in vitro* and *in vivo* models in the frame of a research project with the goal of developing of novel copper(II) complexes with potential anticancer actions. In this sense, CuHL caused concentration-dependent cytotoxicity on 2D (monolayer) and 3D (spheroids) cultures derived from human OS cells (MG-63), showing stronger anticancer activity than CDDP on both cellular systems ($IC_{50(CuHL)}$ 2D: 2.1 ± 0.3 μM; $IC_{50(CDDP)}$ 2D: 39.0 ± 1.8 μM $IC_{50(CuHL)}$ 3D: 9.1 ± 1.0 μM $IC_{50(CDDP)}$ 3D: 65.1 ± 5.6 μM).

According to Santini et al., copper complexes with IC_{50} values < 10 μM can be classified as potent anticancer agents [40]. We have previously studied and reported a series of copper complexes containing hydrazones as ligands, including [$CuHL^1$] [27], [$Cu(L^1)$(*o*-phen)] and [$Cu(HL^1)$(bipy)](NO_3) [33].

In these compounds, the *N*-acylhydrazone ligand (H_2L^1), 4-hydroxy-N'E) 2-hydroxy-3-methoxybenzylidene]benzohydrazide), coordinates through its ONO donor atoms, as tridentate monoanion $(HL^1)^-$ or as dianion $(L^1)^{2-}$. The co-ligands, bipy (2,2′ bipyridine) and *o*-phen (1,10 phenanthroline) interact with de metal center as bidentate, through the heterocycle nitrogen atoms. These copper(II) compounds showed IC_{50} values lower than 10 μM on MG-63 cells but none of them have the same anticancer potency thatCuHL (see Table 1). Vanco et al. published a series of copper(II) complexes-pomiferin and phenantrolines derivatives with interesting anticancer activity on HOS cells (IC_{50} from 3 to 25 μM) [41]. Nevertheless, copper(II) compounds with saccharinate and glutamine exhibit low anticancer activity over MG-63 cell line showing IC_{50} values around 300 μM [26].

Moreover, cell death studies demonstrated that CuHL inhibits cell proliferation and conveys cells to apoptosis. Also, the compound showed great genotoxicity in the low micromolar range (0.5–1.5 μM), evaluated by comet assay. The proteomic analysis showed that the expression of 27 proteins was heavily altered in MG-63 cell cultures after the CuHL treatment. Response to unfolded protein was the most affected biological process but cellular response to heat chaperone cofactor-dependent protein refolding and ATP metabolic processes were affected too.

Up-regulated proteins by CuHL, such as HSP70, HSP105, and BAG3 (Co-chaperone for HSP70) have a key role on carriage of novel polypeptides, stimulation of proteolysis of misfolded proteins and protection of the proteome from stress. In agreement with these results, DNAJB1 and DNAJB4 which have a function of stimulates ATPase activity of HSP70 are up-regulated too. Besides, CuHL up-regulates at ATP6V1C1 which has a function in the maintenance of the pH of intracellular and regulates the actin arrangement in cancer cells promoting metastasis.

On the other hand, CuHL down-regulates relevant proteins related to cell growth and metabolism such us SDHA, GFM1 and pyruvate kinase. These results infer that complex reduces the cell viability and cell proliferation inhibiting ATP production. Moreover, the complex decreases the levels of DNA polymerase that it is involved in DNA replication and DNA repair. This finding is in agreement with comet assay results, postulating that DNA replication inhibition could be a key mechanism of action related to the potent anticancer activity exerted by CuHL. In this sense, it is important to highlight that CuHL down-regulates the thioredoxin-1 (TXNL1, also known as thioredoxin-related 32 kDa protein, TRP32). This protein participates in the regulation of oxidative stress, which protects cells from ROS damage via redox balance [42]. Besides, overexpression of TXNL1 is closely correlated with the initiation of various tumors and it is associated with poor prognosis and aggressive clinicopathological characteristics [43]. In particular, the overexpression of TXNL1 confers resistance to oxidant-induced apoptosis in human OS cells [44]. TXNL1 acts as a pro-tumor protein with a role in the growth signals of cancer cells so is considered an important target in cancer therapy [45]. In this way, gold and ruthenium compounds inhibit indirectly the action and activity of thioredoxin-1 through the inhibition of thioredoxin-1 reductase [46–48].

Moreover, with the aim of assessing its activity *in vivo*, we carried out a protocol with immunosuppressed mice bearing human OS xenografts. Sustained use of CuHL for one month at a dose of 2 mg/kg i.p. significantly attenuated xenograft growth and progression, modulating mitotic rates and enhancing necrosis. Administration of reference metallodrug CDDP at an equivalent dose failed to inhibit OS growth, showing no therapeutic benefits at all.

It is important to highlight that no histopathological alterations or important signs of toxicity were observed in liver or brain tissue, and non-significant increases in alanine aminotransferase and aspartate aminotransferase levels were observed in CuHL-treated animals. In this way, total protein, creatinine, and bilirubin levels remain unaltered. However, a significant drop in the monocyte count was observed in CuHL-treated mice (102.4 ± 47.2 versus 17.3 ± 7.5 for control and CuHL, respectively). In order to continue with the development of CuHL as a promising adjuvant therapeutic tool for the management of OS, further in vivo studies assessing its efficacy on disease progression as well as its associated toxicity are mandatory.

Considering the selectivity and antitumor action of CuHL and the non-existent alternatives in the treatment of OS, our findings show that is an attractive and potential candidate for future anticancer therapies.

Authors' contributions

Lucia M. Balsa contributed in study design and conception, execution of the experiments, data analysis and interpretation, and manuscript writing; Luisina M. Solernó; executed in vivo experiments; Maria R. Rodriguez, Beatriz S. Parajón-Costa and Ana C. Gonzalez-Baró; participated in the synthesis, characterization of CuHL and manuscript revisión; Daniel F. Alonso, Juan Garona and Ignacio E. León participated in the conception and design, financial support, interpretation of study, and supervised all of the experiments. All authors approved the submission of the final manuscript.

Declaration of competing interest

The authors declare the following financial interests/personal relationships which may be considered as potential competing interests: Ignacio Esteban Leon reports was provided by UNLP. We have no conflicts of interest to disclose.

Data availability

Data will be made available on request.

Acknowledgement

This work was supported by CONICET (PIP 2051), UNLP (X053), ANPCyT (PICT 2019-2322 and PICT 2017-2056), INC (2018–2021) and

UNQ (PUNQ 1297-19).

AGB, BPC, DA, IEL, JG are members of the Research Career of CONICET. LMB, LMS, MRR have a fellowship from CONICET.

Appendix A. Supplementary data

Supplementary data to this article can be found online at https://doi.org/10.1016/j.cbi.2023.110685.

References

[1] F. Bray, J. Ferlay, I. Soerjomataram, R.L. Siegel, L.A. Torre, A. Jemal, Global cancer statistics 2018: GLOBOCAN estimates of incidence and mortality worldwide for 36 cancers in 185 countries, CA, Cancer J. Clin. 68 (2018) 394–424, https://doi.org/10.3322/caac.21492.

[2] R. Gorlick, C. Khanna, Osteosarcoma, J. Bone Miner. Res. 25 (2010) 683–691, https://doi.org/10.1002/jbmr.77.

[3] R.S. Benjamin, Adjuvant and neoadjuvant chemotherapy for osteosarcoma: a historical perspective, Adv. Exp. Med. Biol. 1257 (2020) 1–10, https://doi.org/10.1007/978-3-030-43032-0_1.

[4] C. Meazza, P. Scanagatta, Metastatic osteosarcoma: a challenging multidisciplinary treatment, Expert Rev. Anticancer Ther. 16 (2016) 543–556, https://doi.org/10.1586/14737140.2016.1168697.

[5] F. Moreno, W. Cacciavillano, M. Cipolla, M. Coirini, P. Streitenberger, J. López Martí, M. Palladino, M. Morici, M. Onoratelli, G. Drago, A. Schifino, M. Cores, A. Rose, J. Jotomliansky, M. Varel, M. García Lombardi, Childhood Osteosarcoma: Incidence and Survival in Argentina. Report from the National Pediatric Cancer Registry, ROHA Network 2000-2013, Pediatr. Blood Cancer, vol. 64, 2017, https://doi.org/10.1002/PBC.26533.

[6] M. Hanif, C.G. Hartinger, Anticancer metallodrugs: where is the next cisplatin? Future Med. Chem. 10 (2018) 615–617, https://doi.org/10.4155/fmc-2017-0317.

[7] M. Abid, F. Shamsi, A. Azam, Ruthenium complexes: an emerging ground to the development of metallopharmaceuticals for cancer therapy, Mini Rev. Med. Chem. 16 (2016) 772–786. http://www.ncbi.nlm.nih.gov/pubmed/26423699.

[8] T.C. Johnstone, K. Suntharalingam, S.J. Lippard, The next generation of platinum drugs: targeted Pt(II) agents, nanoparticle delivery, and Pt(IV) prodrugs, Chem. Rev. 116 (2016) 3436–3486, https://doi.org/10.1021/acs.chemrev.5b00597.

[9] D. Wang, S.J. Lippard, Cellular processing of platinum anticancer drugs, Nat. Rev. Drug Discov. 4 (2005) 307–320, https://doi.org/10.1038/nrd1691.

[10] L.I.E. Balsa Lucia M, J. Baran Enrique, Copper complexes as antitumor agents: in vitro and in vivo evidence, Curr. Med. Chem. 30 (2023) 510–557.

[11] S. Thota, D.A. Rodrigues, D.C. Crans, E.J. Barreiro, Ru(II) compounds: next-generation anticancer metallotherapeutics? J. Med. Chem. 61 (2018) 5805–5821, https://doi.org/10.1021/acs.jmedchem.7b01689.

[12] D. Denoyer, S.A.S. Clatworthy, M.A. Cater, 16. Copper complexes in cancer therapy, in: A. Sigel, H. Sigel, E. Freisinger, R.K.O. Sigel (Eds.), Met. Dev. Action Anticancer Agents, De Gruyter, Berlin, Boston, 2018, pp. 469–506, https://doi.org/10.1515/9783110470734-022.

[13] M. Pellei, V. Gandin, L. Marchiò, C. Marzano, L. Bagnarelli, C. Santini, Syntheses and biological studies of Cu(II) complexes bearing bis (pyrazol-1-yl)- and Bis (triazol-1-yl)-acetato heteroscorpionate ligands, Molecules 24 (2019) 1–18, https://doi.org/10.3390/molecules24091761.

[14] L.M. Balsa, M.R. Rodriguez, B.S. Parajón-Costa, A.C. González-Baró, M. J. Lavecchia, I.E. León, Anticancer activity and mechanism of action evaluation of an acylhydrazone Cu(II) complex toward breast cancer cells, spheroids, and mammospheres, ChemMedChem 17 (2022) 1–14, https://doi.org/10.1002/cmdc.202100520.

[15] L.M. Balsa, M.C. Ruiz, L. Santa Maria de la Parra, E.J. Baran, I.E. León, Anticancer and antimetastatic activity of copper(II)-tropolone complex against human breast cancer cells, breast multicellular spheroids and mammospheres, J. Inorg. Biochem. 204 (2020) 110975, https://doi.org/10.1016/j.jinorgbio.2019.110975.

[16] L.M. Balsa, V. Ferraresi-Curotto, M.J. Lavecchia, G.A. Echeverría, O.E. Piro, J. Garcia-Tojal, R. Pis-Diez, A.C. González-Baró, I.E. León, Anticancer activity of a new copper (II) complex with a hydrazone ligand. Structural and spectroscopic characterization, computational simulations and cell mechanistic studies on 2D and 3D breast cancer cell models, Dalton Trans. 50 (2021) 9812–9826.

[17] L.M. Balsa, R. Rodriguez, V. Ferraresi-curotto, B.S. Paraj, A.C. Gonzalez-bar, I.E. Le, Finding new molecular targets of two copper (II) -hydrazone complexes on triple-negative breast cancer cells using mass-spectrometry-based, Quantitative Proteomics (2023) 7531.

[18] P. Levin, M.C. Ruiz, A.I.B. Romo, O.R. Nascimento, A.L. Di Virgilio, A.G. Oliver, A. P. Ayala, I.C.N. Diogenes, I. Leon, L.A. Lemus, Water-mediated reduction of [Cu (dmp) $_2$ (CH $_3$ CN)] $^{2+}$: implications of the structure of a classical complex on its activity as an anticancer drug, Inorg. Chem. Front. (2021), https://doi.org/10.1039/D1QI00233C.

[19] A. Sîrbu, O. Palamarciuc, M.V. Babak, J.M. Lim, K. Ohui, E.A. Enyedy, S. Shova, D. Darvasiová, P. Rapta, W.H. Ang, V.B. Arion, Copper(ii) thiosemicarbazone complexes induce marked ROS accumulation and promote nrf2-mediated antioxidant response in highly resistant breast cancer cells, Dalton Trans. 46 (2017) 3833–3847, https://doi.org/10.1039/c7dt00283a.

[20] M.C. Ruiz, K. Perelmulter, P. Levín, A.I.B. Romo, L. Lemus, M.B. Fogolín, I.E. León, A.L. Di Virgilio, Antiproliferative activity of two copper (II) complexes on colorectal cancer cell models: impact on ROS production, apoptosis induction and NF-κB inhibition, Eur. J. Pharmaceut. Sci. 169 (2022) 106092, https://doi.org/10.1016/J.EJPS.2021.106092.

[21] C. Lu, A. Eskandari, P.B. Cressey, K. Suntharalingam, Cancer stem cell and bulk cancer cell active copper(II) complexes with vanillin schiff base derivatives and naproxen, Chem. Eur J. 23 (2017) 11366–11374, https://doi.org/10.1002/chem.201701939.

[22] K. Laws, G. Bineva-Todd, A. Eskandari, C. Lu, N. O'Reilly, K. Suntharalingam, A copper(II) phenanthroline metallopeptide that targets and disrupts mitochondrial function in breast cancer stem cells, Angew. Chem. Int. Ed. 57 (2018) 287–291, https://doi.org/10.1002/anie.201710910.

[23] a.L. Di Virgilio, I.E. León, C.a. Franca, I. Henao, G. Tobón, S.B. Etcheverry, Cu(Nor) 2·5H2O, a complex of Cu(II) with Norfloxacin: theoretic approach and biological studies. Cytotoxicity and genotoxicity in cell cultures, Mol. Cell. Biochem. 376 (2013) 53–61, https://doi.org/10.1007/s11010-012-1548-8.

[24] Y. Mei, S. Zhang, C. Hu, J. Zhang, M. Yang, Synthesis, characterization, and crystal structures of mononuclear and dinuclear copper(II) complexes derived from similar tridentate Schiff bases, Inorg. Nano-Metal Chem. 47 (2017) 1270–1274, https://doi.org/10.1080/24701556.2017.1284115.

[25] J.F. Cadavid-Vargas, P.M. Arnal, R.D. Mojica Sepúlveda, A. Rizzo, D.B. Soria, A. L. Di Virgilio, Copper complex with sulfamethazine and 2,2'-bipyridine supported on mesoporous silica microspheres improves its antitumor action toward human osteosarcoma cells: cyto- and genotoxic effects, Biometals 32 (2019) 21–32, https://doi.org/10.1007/S10534-018-0154-Y.

[26] J. Cadavid-Vargas, I. Leon, S. Etcheverry, E. Santi, M. Torre, A. Di Virgilio, Copper (II) complexes with saccharinate and glutamine as antitumor agents: cytoand genotoxicity in human osteosarcoma cells, Anti Cancer Agents Med. Chem. 17 (2016) 424–433, https://doi.org/10.2174/1871520616666160513130204.

[27] Y. Burgos-Lopez, J. Del Plá, L.M. Balsa, I.E. León, G.A. Echeverría, O.E. Piro, J. García-Tojal, R. Pis-Diez, A.C. González-Baró, B.S. Parajón-Costa, Synthesis, crystal structure and cytotoxicity assays of a copper(II) nitrate complex with a tridentate ONO acylhydrazone ligand. Spectroscopic and theoretical studies of the complex and its ligand, Inorg. Chim. Acta. 487 (2019) 31–40, https://doi.org/10.1016/j.ica.2018.11.039.

[28] M.R. Rodríguez, L.M. Balsa, O.E. Piro, G.A. Etcheverría, J. García-Tojal, R. Pis-Diez, I.E. León, B.P. Parajón-Costa, A.C. González-Baró, Synthesis, crystal structure, spectroscopic characterization, DFT calculations and cytotoxicity assays of a new Cu(II) complex with an acylhydrazone ligand derived from thiophene, Inorganics 9 (2021) 9, https://doi.org/10.3390/inorganics9020009.

[29] N.P. Singh, M.T. McCoy, R.R. Tice, E.L. Schneider, A simple technique for quantitation of low levels of DNA damage in individual cells, Exp. Cell Res. 175 (1988) 184–191. http://www.ncbi.nlm.nih.gov/pubmed/3345800. (Accessed 26 January 2015).

[30] I.E. León, J.F. Cadavid-Vargas, A. Resasco, F. Maschi, M.A. Ayala, C. Carbone, S. B. Etcheverry, In vitro and in vivo antitumor effects of the VO-chrysin complex on a new three-dimensional osteosarcoma spheroids model and a xenograft tumor in mice, JBIC, J. Biol. Inorg. Chem. 21 (2016) 1009–1020, https://doi.org/10.1007/s00775-016-1397-0.

[31] A.I. Matesanz, E. Jimenez-Faraco, M.C. Ruiz, L.M. Balsa, C. Navarro-Ranninger, I. E. León, A.G. Quiroga, Mononuclear Pd(ii) and Pt(ii) complexes with an α-N-heterocyclic thiosemicarbazone: cytotoxicity, solution behaviour and interaction *versus* proven models from biological media, Inorg. Chem. Front. 5 (2018) 73–83, https://doi.org/10.1039/C7QI00446J.

[32] M.C. Ruiz, J. Kljun, I. Turel, A.L. Di Virgilio, I.E. León, Comparative antitumor studies of organoruthenium complexes with 8-hydroxyquinolines on 2D and 3D cell models of bone, lung and breast cancer, Metallomics 11 (2019) 666–675, https://doi.org/10.1039/c8mt00369f.

[33] Y. Burgos-López, L.M. Balsa, O.E. Piro, I.E. León, J. García-Tojal, G.A. Echeverría, A.C. González-Baró, B.S. Parajón-Costa, Tridentate acylhydrazone copper(II) complexes with heterocyclic bases as coligands. Synthesis, spectroscopic studies, crystal structure and cytotoxicity assays, Polyhedron 213 (2022) 115621, https://doi.org/10.1016/j.poly.2021.115621.

[34] M. Hassan, H. Watari, A. AbuAlmaaty, Y. Ohba, N. Sakuragi, Apoptosis and molecular targeting therapy in cancer, BioMed Res. Int. 2014 (2014) 1–23, https://doi.org/10.1155/2014/150845.

[35] M. Van Engeland, L.J.W. Nieland, F.C.S. Ramaekers, B. Schutte, C.P. M. Reutelingsperger, Annexin V-affinity assay: a review on an apoptosis detection system based on phosphatidylserine exposure, Cytometry 31 (1998) 1–9, https://doi.org/10.1002/(SICI)1097-0320(19980101)31:1<1::AID-CYTO1>3.0.CO;2-R.

[36] I. Leon, J.F. Cadavid-Vargas, A.L. Di Virgilio, S. Etcheverry, I.E. León, J.F. Cadavid-Vargas, A.L. Di Virgilio, S. Etcheverry, I. Leon, J.F. Cadavid-Vargas, A.L. Di Virgilio, S. Etcheverry, Vanadium, ruthenium and copper compounds: a new class of nonplatinum metallodrugs with anticancer activity, Curr. Med. Chem. 24 (2017) 112–148, https://doi.org/10.2174/0929867323666160824162546.

[37] M.R. Rodríguez, J. Del Plá, L.M. Balsa, I.E. León, O.E. Piro, G.A. Echeverría, J. García-Tojal, R. Pis-Diez, B.S. Parajón-Costa, A.C. González-Baró, Cu(ii) and Zn (ii) complexes with a poly-functional ligand derived from: O -vanillin and thiophene. Crystal structure, physicochemical properties, theoretical studies and cytotoxicity assays against human breast cancer cells, New J. Chem. 43 (2019) 7120–7129, https://doi.org/10.1039/c8nj06274a.

[38] Y. Tu, C. Chen, J. Pan, J. Xu, Z.G. Zhou, C.Y. Wang, The ubiquitin proteasome pathway (UPP) in the regulation of cell cycle control and DNA damage repair and its implication in tumorigenesis, Int. J. Clin. Exp. Pathol. 5 (2012) 726–738.

[39] M. Červinka, The role of mitochondria in apoptosis induced in vitro, Gen. Physiol. Biophys. 18 (1999) 33–40, https://doi.org/10.1146/annurev-genet-102108-134850. The.

[40] C. Santini, M. Pellei, V. Gandin, M. Porchia, F. Tisato, C. Marzano, Advances in copper complexes as anticancer agents, Chem. Rev. 114 (2014) 815–862, https://doi.org/10.1021/cr400135x.
[41] J. Vančo, Z. Trávníček, J. Hošek, T. Malina, Z. Dvořák, Copper(II) complexes containing natural flavonoid pomiferin show considerable in vitro cytotoxicity and anti-inflammatory effects, Int. J. Mol. Sci. 22 (2021) 7626, https://doi.org/10.3390/IJMS22147626.
[42] J.M. Zhao, T.G. Qi, The role of TXNL1 in disease: treatment strategies for cancer and diseases with oxidative stress, Mol. Biol. Rep. 48 (2021) 2929–2934, https://doi.org/10.1007/S11033-021-06241-Z.
[43] W. Shang, Z. Xie, F. Lu, D. Fang, T. Tang, R. Bi, L. Chen, L. Jiang, Increased thioredoxin-1 expression promotes cancer progression and predicts poor prognosis in patients with gastric cancer, Oxid. Med. Cell. Longev. (2019), https://doi.org/10.1155/2019/9291683, 2019.
[44] Y. Chen, J. Cai, T.J. Murphy, D.P. Jones, Overexpressed human mitochondrial thioredoxin confers resistance to oxidant-induced apoptosis in human osteosarcoma cells, J. Biol. Chem. 277 (2002) 33242–33248, https://doi.org/10.1074/JBC.M202026200.
[45] M. Jovanović, A. Podolski-Renić, M. Krasavin, M. Pešić, The role of the thioredoxin detoxification system in cancer progression and resistance, Front. Mol. Biosci. 9 (2022), https://doi.org/10.3389/FMOLB.2022.883297.
[46] A. Bindoli, M.P. Rigobello, G. Scutari, C. Gabbiani, A. Casini, L. Messori, Thioredoxin reductase: a target for gold compounds acting as potential anticancer drugs, Coord. Chem. Rev. 253 (2009) 1692–1707, https://doi.org/10.1016/j.ccr.2009.02.026.
[47] J. Kladnik, J.P.C. Coverdale, J. Kljun, H. Burmeister, P. Lippman, F.G. Ellis, A. M. Jones, I. Ott, I. Romero-Canelón, I. Turel, Organoruthenium complexes with benzo-fused pyrithiones overcome platinum resistance in ovarian cancer cells, Cancers 13 (2021), https://doi.org/10.3390/CANCERS13102493.
[48] E. Schuh, C. Pflüger, A. Citta, A. Folda, M.P. Rigobello, A. Bindoli, A. Casini, F. Mohr, Gold(I) carbene complexes causing thioredoxin 1 and thioredoxin 2 oxidation as potential anticancer agents, J. Med. Chem. 55 (2012) 5518–5528, https://doi.org/10.1021/JM300428V/SUPPL_FILE/JM300428V_SI_001.PDF.